Heliyon 9 (2023) e14810

Contents lists available at ScienceDirect

Heliyon

journal homepage: www.cell.com/heliyon

Research article

Novel roles for HMGA2 isoforms in regulating oxidative stress and sensitizing to RSL3-Induced ferroptosis in prostate cancer cells

Taaliah Campbell [a,1], Ohuod Hawsawi [a,1], Veronica Henderson [a], Precious Dike [b], Bor-Jang Hwang [b], Yusuf Liadi [b], ElShaddai Z. White [a], Jin Zou [a], GuangDi Wang [c], Qiang Zhang [c], Nathan Bowen [a], Derrick Scott [d], Cimona V. Hinton [a], Valerie Odero-Marah [b,*]

[a] Center for Cancer Research and Therapeutic Development, Department of Biological Sciences, Clark Atlanta University, Atlanta, GA, 30314, USA
[b] Center for Urban Health Disparities Research and Innovation, Department of Biology, Morgan State University, Baltimore, MD, 21251, USA
[c] Department of Chemistry, Xavier University, New Orleans, LA, 70125, USA
[d] Department of Biological Sciences, Delaware State University, Dover, DE, 19901, USA

ARTICLE INFO

Keywords:
HMGA2
Truncated HMGA2
Oxidative stress
Ferroptosis
Prostate cancer

ABSTRACT

Oxidative stress is increased in several cancers including prostate cancer, and is currently being exploited in cancer therapy to induce ferroptosis, a novel nonapoptotic form of cell death. High mobility group A2 (HMGA2), a non-histone protein up-regulated in several cancers, can be truncated due to chromosomal rearrangement or alternative splicing of HMGA2 gene. The purpose of this study is to investigate the role of wild-type vs. truncated HMGA2 in prostate cancer (PCa). We analyzed the expression of wild-type *vs*. truncated HMGA2 and showed that prostate cancer patient tissue and some cell lines expressed increasing amounts of both wild-type and truncated HMGA2 with increasing tumor grade, compared to normal epithelial cells. RNA-Seq analysis of LNCaP prostate cancer cells stably overexpressing wild-type HMGA2 (HMGA2-WT), truncated HMGA2 (HMGA2-TR) or empty vector (Neo) control revealed that HMGA2-TR cells exhibited higher oxidative stress compared to HMGA2-WT or Neo control cells, which was also confirmed by analysis of basal reactive oxygen species (ROS) levels using 2′, 7′-dichlorofluorescin diacetate (DCFDA) dye, the ratio of reduced glutathione/oxidized glutathione (GSH/GSSG) and NADP/NADPH using metabolomics. This was associated with increased sensitivity to RAS-selective lethal 3 (RSL3)-induced ferroptosis that could be antagonized by ferrostatin-1. Additionally, proteomic and immunoprecipitation analyses showed that cytoplasmic HMGA2 protein interacted with Ras GTPase-activating protein-binding protein 1 (G3BP1), a cytoplasmic stress granule protein that responds to oxidative stress, and that G3BP1 transient knockdown increased sensitivity to ferroptosis even further. Endogenous knockdown of HMGA2 or G3BP1 in PC3 cells reduced proliferation which was reversed by ferrostatin-1. In conclusion, we show a novel role for HMGA2 in oxidative stress, particularly the truncated HMGA2, which may be a therapeutic target for ferroptosis-mediated prostate cancer therapy.

* Corresponding author. Center for Urban Health Disparities Research and Innovation, Department of Biology, Morgan State University, Baltimore, MD, 21251, USA.
E-mail addresses: taaliah.campbell@students.cau.edu (T. Campbell), ohawsawi@augusta.edu (O. Hawsawi), valerie.odero-marah@morgan.edu (V. Odero-Marah).
[1] These authors contributed equally to this work.

https://doi.org/10.1016/j.heliyon.2023.e14810
Received 1 November 2022; Received in revised form 9 March 2023; Accepted 17 March 2023
Available online 7 April 2023

1. Introduction

High mobility group A2 (HMGA2) is a non-histone protein that acts as an architecture transcription factor influencing structural aspects of enhancesomes through a network of protein:protein and protein:DNA interactions which leads to transcriptional regulation of target genes [1,2]. Studies have shown that an elevated level of HMGA2 protein is associated with several types of cancer, including pancreatic carcinoma [3], lung carcinomas [4], carcinoma of oral cavity [5], and prostate cancer (PCa) [6]. The truncated version of HMGA2 is caused by a translocation breakpoint at the third exon in the gene, which leads to the deletion of a section of its *C*-terminus and 3′UTR. [7], or via alternative splicing [8]. Overexpression of the truncated form of HMGA2 has already been observed in uterine leiomyoma cancer [9] and myeloid leukemia [10], yet its part in prostate cancer is still unknown. Moreover, its mode of action has not been studied previously.

Excessive generation of reactive oxygen species (ROS) leads to oxidative stress [11], which has been associated with PCa progression [12,13]. Cytosolic NADPH oxidases (NOX) are considered as the major source of ROS generation, while mitochondrial oxidative metabolisms are also another source; ROS generated by NOX activation can reduce the mitochondrial membrane potential, leading to mitochondrial ROS formation and subsequent activation of NOX, thus, these processes increase total intracellular ROS production in a vicious circle [14]. The redox balance between mitochondrial reduced glutathione (GSH) and its oxidized form (GSSG) is maintained with the help of other reduced agents such as NADPH [15]. The GSH/GSSG ratio is a commonly used indicator of oxidative stress. Generally, this ratio is 1:100, but it can reduce to 10:1 and even 1:1 in times of stress [16]. In response to oxidative stress, the GTPase-activating protein SH3 domain-binding protein 1 (G3BP1) has been found to initiate the formation of stress granules in the cytoplasm [17]. Overexpression of G3BP1 has been observed in a number of cancers including gastric cancer, breast cancer and renal cell carcinoma [18].

Ferroptosis is a form of nonapoptotic cell death that was recently discovered, and unlike autophagy or apoptosis, relies on iron and ROS, thus, oxidative stress pathways are responsible partly for ferroptosis [19]. Specifically, ferroptosis, a specific type of cell death caused in part by oxidative stress is mediated by the accumulation of lipid peroxides, which are formed as a result of ROS-induced damage to cell membrane lipids [19]. This accumulation leads to the dysfunction of cell membrane and ultimately cell death. Some studies even suggest that ferroptosis may play a role in the development of certain diseases, such as cancer, neurodegeneration, and cardiovascular disease [20]. Ferroptosis can be promoted by both membrane-mediated ROS driven by NOX and mitochondrial-mediated ROS, or by disarming the antoxidant defense system [21]. Moreover, erastin and RSL3 act as ferroptosis indcuers to promote ferroptotic cell death. Speifically, RSL3 inhibits glutathione peroxidase 4 (GPX4), and loss or inhibition of GPX4 leads to induction of ferroptosis in cencer cells [22]. Interestingly, ferroptosis inducers such as erastin and RSL3 are being explored for combination therapy with chemotherapeutic agents such as cisplatin, temozolomide and enzalutamide in lung cancer, glioblastoma and prostate cancer, respectively [22–24].

The aim of this study is to investigate the mechanistic role of truncated HMGA2 in relation to PCa progression and compare it to wild-type HMGA2. Although we have previously shown that truncated HMGA2 increases cell proliferation and migration [25], we did not examine a mechanism.

2. Materials and methods

2.1. Cell culture and reagents

Prostate cancer cell lines (RWPE1, 22Rv1, DU145, PC3) were obtained from the American Type Culture Collection (Manassas, VA). C4-2, ARCaP-E and ARCaP-M cells were a kind gift from Dr. Leland Chung (Cedars Sinai Medical Center, Los Angeles, CA). LNCaP cells overexpressing either wild-type HMGA2 (HMGA2-WT), truncated HMGA2 (HMGA2-TR), or Neo control (Neo) were generated previously [25]. The cells were grown in RPMI-1640 (Lonza, Alpharetta, GA) supplemented with 10% (v/v) FBS from (Atlanta biological, Flowery Branch, GA), 50 μg/ml penicillin, and 100 μg/ml streptomycin, except for RWPE1 cells which were grown in keratinocyte-SFM media supplemented with keratinocyte supplements (ThermoFisher Scientific, Grand Island, NY). All cells were maintained at 37 °C with 5% CO_2 in a humidified incubator. Nitrocellulose membranes and iodoacetamide were from Bio-Rad (Hercules, CA). CM-DCFDA was from Invitrogen (Eugene, OR). Mouse monoclonal *anti*-α-tubulin was purchased from Millipore-Sigma (Burlington, MA). Anti-mouse G3BP1 antibody was purchased from Santa Cruz Biotechnology (Santa Cruz, CA). Goat monoclonal *anti*-HMGA2 was purchased from R&D Systems (Minneapolis, MN) for immunofluorescence and *anti*-HMGA2 (ThermoFisher, Waltham, MA) for Western blot analyses. The protease inhibitor cocktail was from Roche Molecular Biochemicals (Indianapolis, IN). Smartpool small interfering RNA (siRNA) for G3BP1 and control siRNA and Dharmafect 1 transfection reagent were purchased from Horizon Discovery (Boyertown, PA). MTS assay was from Promega (Madison, WI). HRP-conjugated sheep anti-mouse and donkey anti-rabbit secondary antibodies were purchased from GE Healthcare Life Sciences (Marlborough, MA) and donkey anti-goat secondary antibody was purchased from Santa Cruz Biotechnology. RSL3 and ferrostatin-1 were purchased from ApexBio (Houston, TX).

2.2. Cell culture and reagents

Prostate tumors with matched normal tissues were obtained from Protein biotechnologies, Ramona, CA. Protein Biotechnologies Inc. provides pharmaceutical, biotechnology, government, and academic institutions with human clinical specimen derivatives. Tissues are obtained through a global network of participating medical centers that employ IRB approved protocols and strict ethical

guidelines to ensure patient confidentiality and safety.

Prostate normal and cancer tissue cDNA array (TissueScan, Prostate Cancer cDNA Array III- CAT#: HPRT103) was purchased from OriGene (Rockville, MD). All samples were collected under IRB approved protocols. All human subjects are fully informed and are explicitly asked for their consent to future research use of their samples, even in cases where such uses are unknown. De-identified and coded patient numbers (Case IDs) ensure the privacy of donors in accordance with the Health Insurance Portability and Accountability Act (HIPPA).

2.3. Prostate patient tissue lysates

Prostate tumors with matched normal tissues were obtained from Protein biotechnologies (Ramona, CA). Samples utilized were benign prostatic fibrosis (cat# T3-003-T-1), normal prostate tissue (cat# T3-020-N-1, T3-022-N-1), prostatic adenocarcinoma Grade I Gleason 5 (cat# T3-023-N-1), prostatic adenocarcinoma GradeII Gleason 7 (cat# T3-024-N-1), prostatic adenocarcinoma Grade III Gleason 9 (cat# T3-025-N-1), prostatic adenocarcinoma Grade I Gleason 4 (cat# T3-033-N-1), prostatic adenocarcinoma Grade II Gleason 5 (cat#T3-036-N-1), prostatic adenocarcinoma Grade III Gleason 9 (cat# T3-037-N-1). Identical procedures are used to prepare all patient samples. Specimens are flash frozen to −120 °C within 5 min of removal to minimize autolysis, oxidation, and protein degradation. Tissue specimens are homogenized in modified RIPA buffer (PBS, pH 7.4, 1 mM EDTA, and protease inhibitors) to obtain the soluble proteins, and centrifuged to clarify.

2.4. Western blot analysis

Total protein cell lysis from 1X10 [6] cells was collected in 1X modified RIPA buffer (50 mM Tris pH 8.0, 150 mM NaCl, 0.02% NaN_3, 0.1% SDS, 1% NP-40, 0.5% sodium deoxycholate) containing 1.5X protease inhibitor cocktail, 1 mM phenylmethylsulfonyl fluoride (PMSF), and 1 mM sodium orthovanadate inhibitor. The lysates were freeze-thawed at −80 °C/4 °C for three cycles, and then centrifuged at 13,500 rpm for 30 min at 4 °C. The supernatants were collected, and the proteins were quantified using BCA assay (Promega, Madison, WI). For each sample, 30–50 μg of the cell lysates were resolved using 10% SDS-PAGE gel and transferred to nitrocellulose membranes (Bio-Rad Laboratories, Hercules, CA). Membranes were blocked in 5% milk (TBS-T with 0.05% Tween-20) or 3% BSA (Buffer#8: 25 mM Tris, 0.5 M NaCl, 0.05% Tween 20, pH 7.4: for HMGA2) and incubated with primary antibody. Subsequently, the membranes were incubated with secondary antibody, developed using Luminata Forte ECL prime reagent (Milipore, Billerica, MA), and visualized by AmershamTM Imager to detect the protein expression. The membranes were stripped using Restore Western blot stripping buffer (Pierce Biotechnology, Rockford, IL) prior to re-probing with a different antibody.

2.5. Quantitative real-time PCR

The human TissueScan quantitative PCR (qPCR) Prostate Cancer Array III (HPRT103; OriGene, Rockville, MD) which is provided as cDNA was utilized for determining the mRNA expression of HMGA2-WT and HMGA2-TR in clinical samples. This array contains 48 tissues covering 9 normal tissues and 39 prostate cancer tissues (18-Stage II, 19-Stage III, and 2-Stage IV). The primers synthesized using IDT website include HMGA2-WT, Forward 5′- GATCCAACTGCTGCTGAGGT-3'; Reverse 5′- AGGCAGACCTAGGAAATGGC-3'; HMGA2-TR, Forward 5′ GCCGTCTTCAGCCCAGG-3'; Reverse 5′-CCTAGGTCTGCCTCTTGGCCGT-3'. Relative quantification of HMGA2-WT and HMGA2-TR expression was normalized to housekeeping gene β-actin (forward- and reverse-) supplied with the array kit using the ΔCT method. Gene expression was defined as the threshold cycle number (C_T). Mean fold change in expression of the target genes were calculated using the comparative C_T method (RU; $2^{-\Delta Ct}$).

2.6. Immunofluorescent staining

5 × 10 [3] cells were plated into 16 well chamber slides (Bio-Tek, Nunc, Winooski, VT), fixed with methanol/ethanol 1:1 vol for 5 min, and blocked with 5% goat serum (Thermo Fisher; Minneapolis, MN). Subsequently, slides were incubated with primary antibody in Dako antibody diluent solution (Dako, Camarillo, CA) for 1 h at room temp. Slides were washed with 1X TBS-T (Dako, Camarillo, CA), then incubated with secondary antibody (anti-rabbit Oregon green 488 or anti-mouse Alexa red 594 from Invitrogen, Carlsbad, CA) in the dark for 1 h at room temp. Slides were washed with 1X TBS-T and double deionized water and subsequently counterstained with DAPI (1 μg/ml, Santa Cruz Biotechnology, Santa Cruz, CA). Slides were mounted using Fluorogel mounting medium (Electron Microscopy Sciences, Hatfield, PA). Fluorescence microscopy was performed using Zeiss microscope and AxiovisionRel 4.8 software.

2.7. Immunoprecipitation (IP)

2 × 10 [6] cells were plated overnight followed by subcellular fractionations for LNCaP cells overexpressing HMGA2 (WT and TR) per the manufacturer's instructions (Subcellular Protein Fractionation Kit; Thermo Scientific; Waltham, MA). Briefly, cells at 80–90% confluence were lysed in a series of buffers containing protease inhibitors (25X) with CERI (100 μl), CERII (5.5 μl), or NER (50 μl). Whole cell lysate from LNCaP HMGA2-WT and LNCaP HMGA2-TR cells were also collected. Additionally, centrifugation steps were performed to obtain a non-nuclear fraction and an intact nuclear pellet, followed by further lysing to isolate the nuclear fraction. We have previously shown that wild-type HMGA2 is nuclear/cytoplasmic while truncated HMGA2 in LNCaP cells was predominantly cytoplasmic [26]. Therefore, 1 mg of nuclear or cytoplasmic fraction from LNCaP HMGA2-WT, and 1 mg cytoplasmic fraction for

LNCaP HMGA2-TR was incubated with 5 μg HMGA2 antibody overnight at 4 °C on a rocking platform. Protein A/G PLUS Agarose Beads (1:10, Santa Cruz Biotechnology) were added to each sample for 2 h at 4 °C with gentle agitation. Beads were washed 2X in 1X PBS (max speed for 5 min at 4 °C), boiled in laemmli sample buffer for 5 min, and supernatant run on 10% SDS-PAGE followed by Western blot with *anti*-G3BP1 (1:500).

2.8. Transfection with G3BP1 or HMGA2 siRNA

Transient transfections as per the manufacturer's instructions were performed with 30 nM of non-silencing ON-TARGET plus SMARTpool control siRNA (Catalog # D-001810-10-05), HMGA2 siRNA (Catalog # L-013495-00-0005) or G3BP1 siRNA (Catalog# L-012099-00-0005) obtained from Thermo Scientific - Dharmacon, Lafayette, CO. Briefly, cells were plated at density of 1.5×10 [5] cells in 6-well plates in RPMI media with 10% FBS, without antibiotic, and incubated overnight at 37 °C. Smartpool small interfering RNAs (30 nM) for G3BP1, HMGA2 or control siRNA (30 nM), were transfected into LNCaP HMGA2-WT or -TR using DharmaFECT1 or PC3 cells using DharmaFECT2 transfection reagent from Dharmacon (Chicago, IL) following manufacturer's recommendations. After 48 or 72 h cells were processed for immunofluorescence, cell viability, and Western blot analysis.

2.9. Metabolomics

2.9.1. Metabolite extraction and MS sample preparation

Metabolite extraction was performed as described previously [27]. LNCaP cells overexpressing HMGA2 WT, TR or Neo were washed twice with cold PBS and polar metabolites were subsequently extracted with cryogenically cold 80% methanol/water mixture (LC-MS grade water (Sigma, MO, USA) and LC-MS grade methanol (Fischer Scientific, PA, USA) were used). Methanol extracted samples were dried using a speed vacuum evaporator (Savant Speed Vac® Plus, Thermo Electron Corporation, USA) to evaporate the methanol and lyophilized by using a freeze dry system (Labconco, Kansas City, USA) to remove the water.

2.9.2. LC-MS/MS experiment and analysis

Lyophilized samples were dissolved in equal amounts of LC-MS grade water and applied to LC-MS/MS analysis, using a multiple reaction monitoring (MRM) method by utilizing AB SCIEX 5500 QTRAP, as described previously [27]. Data acquisition was performed by using AnalystTM1.6 software (AB SCIEX) and peaks were integrated by using MultiquantTM (AB SCIEX). Peak areas were normalized by using respective protein concentrations and the resultant peak areas were subjected to relative quantification analyses with MetaboAnalyst 2.0 [28].

2.9.3. RNA-seq analysis

RNA was isolated from LNCaP cells overexpressing HMGA2-WT, HMGA2-TR, and Neo control using the Qiagen kit as per manufacturer's instructions. The concentration and integrity of the RNA using the Nano Drop 2000C Spectrophotometer. Subsequently, extracted RNA was stored at −80 °C until being shipped on dry ice to the Genomic Services Laboratory at Hudson Alpha Discovery (Huntsville, AL) for RNA Seq analysis. Briefly, the mRNA was fragmented and copied into first-strand cDNA, followed by second-strand cDNA synthesis. The cDNA fragments then went through an end repair process, the addition of a single "A" base, and then ligation of the adapters. Subsequently, the products were then purified and enriched with PCR to create final cDNA library which were prepared using the Illumina TruSeq RNA Sample Preparation Kit (Illumina) as dictated by the TruSeq protocol. The libraries were amplified with 15 cycles of PCR and contained TruSeq indexes within the adapters. Finally, amplified library yields were quantified. After KAPA quantification and dilution, the libraries were clustered 4 per lane and sequenced on an Illumina HiSeq200 instrument. Gene Ontology Enrichment and Visualization Tool was applied to analyze enriched gene ontology terms of the HMGA2 gene. These terms include biological processes, cellular components, and molecular functions based on the online platform Gorilla (http://cbl-gorilla.cs.technion.ac.il). Bioinformatic analysis was further conducted to identify differentially expressed genes of HMGA2-WT and HMGA2-TR cells individually compared to LNCaP Neo cells. Outcomes were uploaded into Qiagen's Ingenuity Pathway Analysis (IPA) system for core analysis and then overlaid with the global molecular network in the Ingenuity pathway knowledge base. IPA was performed to identify canonical pathways, functions, and gene networks that are significant to HMGA2 isoforms and to further categorize differentially expressed genes in specific functions.

2.10. Proteomic profiling of LNCaP cells with WT/TR HMGA2 overexpression

2.10.1. Cell lysis, reduction, alkylation, and trypsin digestion

We prepared non-nuclear (cytoplasmic) fraction from LNCaP Neo (control), cytoplasmic fraction from LNCaP HMGA2-TR, and nuclear fraction from LNCaP HMGA2-WT using TheromoFisher Subcellular Protein Fractionation kit, and replicate samples were added into 100 μl of 200 mM TEAB (Sigma-Aldrich, St. Louis, MO). Reduction was performed by adding 5 μl of 200 mM Tris (2-carboxyethyl) phosphine TCEP (Sigma-Aldrich, St. Louis, MO) and incubating for 1 h at 55 °C. Subsequently, alkylation was carried out by adding 5 μl of 375 mM iodoacetamide and incubating for 30 min without light at room temperature. Protein precipitation was performed with 1 ml prechilled acetone overnight at −20 °C. The acetone-precipitated protein pellets were resuspended with 100 μl of 200 mM TEAB, and 2.5 μg of sequencing grade modified trypsin (Promega Corp., Madison, WI) was applied to digest each replicate overnight at 37 °C as previously done [29].

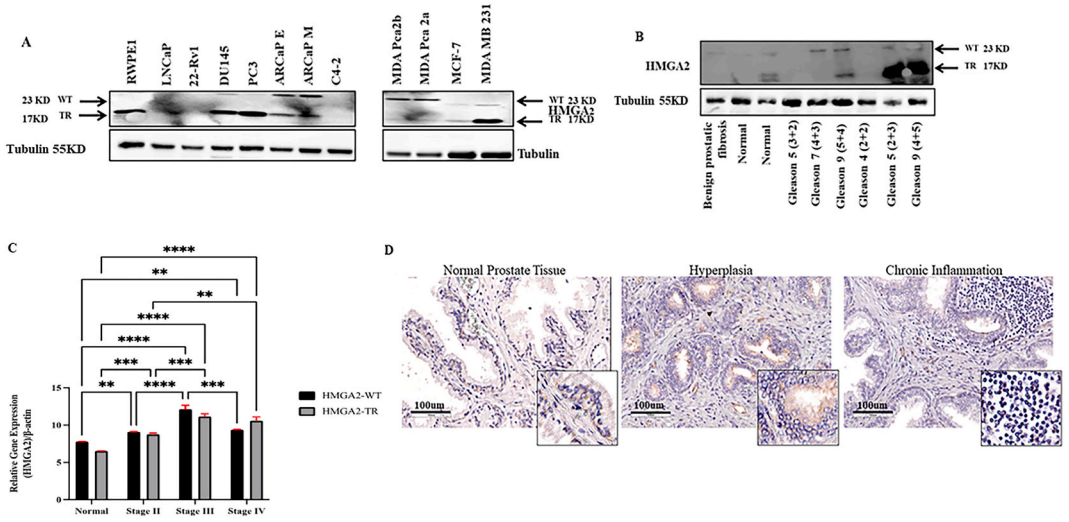

Fig. 1. HMGA2-WT and -TR Expression in PCa and Breast cancer Cell Lines and Patients Tissue
(A) Western blot analysis shows the expression of HMGA2 protein in prostate cancer and breast cancer cell lines, HMGA2-WT displays a higher molecular weight at about 23 KDa while the HMGA2-TR displays a lower molecular of about 17 KDa. (B) Western blot analysis measured the protein levels of both HMGA2-WT and -TR in prostate cancer patient tissue displaying different Stage/Gleason scores. (C) RT-PCR measured the mRNA levels in cDNA array. (D) Immunohistochemical analysis was performed using prostate tissue microarray with HMGA2 antibody in normal prostate tissue, hyperplasia, and chronic inflammation prostate tissue. Scale bar; 100 μm. Magnification 20X, inset 40X. Statistical analysis was conducted utilizing GraphPad Prism; (****$p < 0.0001$, ***$p < 0.001$, **$p < 0.01$). Bars represents SD of the mean. Alpha-tubulin was used as a loading control. Results are representative of 3 independent experiments.

2.10.2. TMT isobaric labeling, fractionation, desalination

According to the manufacturer's protocol, tandem mass tags TMT (Thermo Scientific) with different molecular weights (126–131 Da) (Thermo Scientific, Waltham, MA) were applied as isobaric tags for quantification analysis as previously described [30].

2.10.3. LC-MS/MS analysis, database search, and TMT quantification

Peptides were analyzed on a LTQ-Orbitrap XL (Thermo Scientific) interfaced with an Ultimate 3000 Dionex LC system (Dionex, Sunnyvale, CA) by using high mass resolution to identify peptides and high energy collision dissociation (HCD) to quantify reporter ions as previously described [31]. MS scans were acquired in profile mode and MS/MS scans in centroid mode, respectively. The protein search engine Sequest (Thermo Scientific) was used for peptide matching and protein identification. The minimum number of peptides used for identification and quantification of proteins was one unique peptide. For TMT quantification, the ratios of TMT reporter ion intensities in MS/MS spectra (up to six reporter ions ranging from m/z 126.12 to m/z 131.14) from raw data sets were used to calculate fold changes of proteins between control and HMGA2 wild-type/truncated.

2.11. Reactive oxygen species (ROS) assay

LNCaP Neo, LNCaP HMGA2-WT or HMGA2-TR cells were cultured to approximately 80% confluency. Cells were trypsinized, counted and 1×10 [4] cells resuspended in 20 μM of CM-DCFDA (which measures hydrogen peroxide) and incubated at 37 °C for 1 h. The reaction was stopped on ice and the cells were centrifuged. Cells resuspended in PBS were plated in a 96-well black clear bottom plate and read immediately at 485 nm excitation and 535 nm emission using a BioTek plate reader.

2.12. Cell viability assay

Cell viability was assayed using MTS assay as per manufacturer instructions. Briefly, 1.5×10 [3] cells were plated to each well of a 96 well plate and incubated overnight at 37 °C. The next day, media was removed and treatments performed with either DMSO control or ferroptosis inducer RSL3 (0.12–4 μM) for 72 h, plus or minus ferroptosis inhibitor, Ferrostatin-1 (1 μM). Cell viability was subsequently measured at 490 nm wavelength. For siRNA treatments, control and G3BP1 or HMGA2 siRNA treatments were added to the appropriate wells for 24 h prior to treatment with ferroptosis inducer RSL3 (4 μM) for another 24 h. Cell viability was subsequently measured at 490 nm wavelength using a BioTek plate reader.

2.13. Immunohistochemistry

We examined the expression of HMGA2 in normal, benign, and chronic inflammation human prostate tissue (US BiomaxPR8011a) by immunohistochemistry (IHC). IHC was performed using the Avidin-biotin method as previously described [31]. Images were acquired using the Leica Aperio VERSA.

2.14. Statistical analysis

Results are reported as mean ± SD from 3 experiments. Statistical significance was assessed using GraphPad Prism software by paired Student's t-test and considered significant at $P < 0.05$.

3. Results

3.1. HMGA2 wild-type and truncated expression in higher in prostate cell lines and tissue

We have previously explored the expression of HMGA2 protein in prostate cell lines [25]. We confirmed by Western blot analysis that expression of wild-type HMGA2 is low in RWPE1 normal transformed prostate epithelial cells, but aggressive ARCaP-E/M and MDA-PCa-2a/2b prostate cancer cells express the highest levels of wild-type HMGA2 (approx. 23 kDa), although interestingly, the HMGA2 protein in MDA-PCa-2a/2b is a slightly higher molecular weight (approx. 25 kDa) possibly due to post-translational modifications (Fig. 1A). The lower molecular weight HMGA2-TR (approx. 17 kDa) is relatively high in RWPE1, DU145, PC3 prostate cells and MDA-MB-231 breast cancer cells, moderate in ARCaP-E/M, and low in LNCaP, 22Rv1, C4-2, MDA-PCa-2a/b, and MCF-7 breast cancer cells (Fig. 1A). HMGA2 mRNA and protein expression was further examined in patient tissue. We utilized protein lysate from PCa patient tissue. Results indicate that both HMGA2 isoforms are expressed with increasing levels with PCa gleason grade/stage when compared to normal patients (Fig. 1B). Similar findings are obtained from qPCR utilizing primers specific for either HMGA2-WT or HMGA2-TR (primers generated against exon 4 that is exclusive to truncated due to alternative splicing) in patient mRNA array (Supplemental Fig. 1, Fig. 1C). For further investigation, we stained normal, benign hyperplasia and chronic inflammation prostate tissue with HMGA2 antibody. We observe the cytoplasmic localization of HMGA2 utilizing immunohistochemistry staining for HMGA2, particularly in chronic inflammation tissue, which indicates that HMGA2 is associated with oxidative stress (Fig. 1D). We

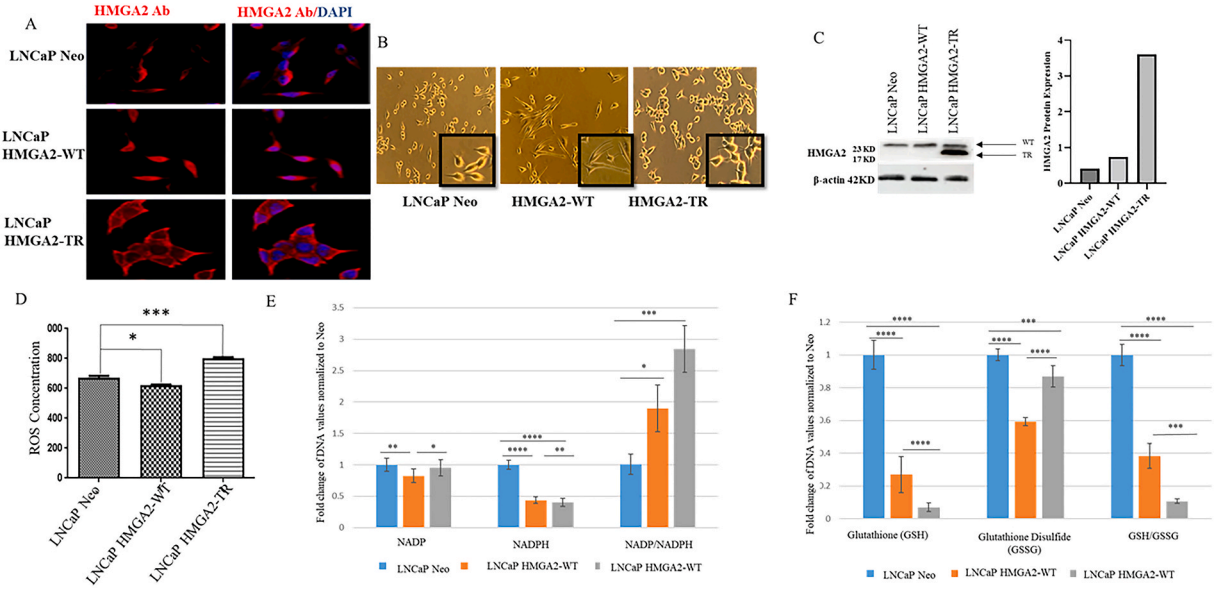

Fig. 2. LNCaP Cells Stably Overexpressing Truncated HMGA2 Display Cytoplasmic Localization and Increased Reactive Oxygen Species
LNCaP cells stably overexpressing wild-type HMGA2 (HMGA2-WT), truncated HMGA2 (HMGA2-TR) or empty vector control (Neo) were assayed by (A) immunofluorescence with *anti*-HMGA2 antibody, and DAPI to stain the nucleus. HMGA2-WT displays a nuclear/cytoplasmic localization while HMGA2-TR is predominantly cytoplasmic. Magnification 40X. (B) Overexpression of HMGA2-WT and HMGA2-TR is associated with morphological changes compared to Neo control as shown by brightfield microscopy. Magnification 20X; Inset 40X. (C) Western blot analysis shows expression of HMGA2 in LNCaP Neo, LNCaP HMGA2-WT, and LNCaP HMGA2-TR with quantification of the blot using Image J (NIH). (D) ROS was measured using DCFDA which shows that HMGA2-TR increases ROS generation. Metabolomics analysis reveals that (E) NADP/NADPH ratio is increased while (F) there is significant decrease in GSH/GSSG ratio in HMGA2-TR compared to HMGA2-WT and Neo. Statistical analysis was done with GraphPad Prism; (****$p < 0.0001$, ***$p < 0.001$, **$p < 0.01$, *$p < 0.05$). Bars represents SD of the mean. Results are representative of 3 independent experiments.

have previously published nuclear expression of HMGA2 in metastatic PCa patient tissue [25]. Therefore, both HMGA2 wild-type and truncated isoforms can be found in PCa patients and increase with tumor progression, while high expression of cytoplasmic HMGA2 is found in prostate tissue displaying chronic inflammation.

3.2. *LNCaP cells stably overexpressing truncated HMGA2 display cytoplasmic localization and increases oxidative stress more than wild-type HMGA2*

As we have previously published [25], we confirm that HMGA2-WT displays nuclear and some cytoplasmic localization while HMGA2-TR overexpression is predominantly cytoplasmic (Fig. 2A). Their morphologies are also distinct from Neo control cells (Fig. 2B). We also confirmed HMGA2 overexpression in LNCaP cells by Western blot analysis (Fig. 2C). Additionally, we measured the ROS levels in these cells which shows a significant increase with the HMGA2-TR, while HMGA2-WT showed decreased levels of ROS compared to Neo control (Fig. 2D). Furthermore, we performed metabolomics analysis with LNCaP cells overexpressing HMGA2- WT, -TR or Neo control followed by samples processing and analysis of mitochondrial oxidative enzymes. The results show that the antioxidant enzyme GSH and GSH/GSSG ratio are reduced in HMGA2-TR, while the NADPH/NADP ratio is significantly higher in HMGA2-TR cells compared to Neo control, moreover, HMGA2-WT had intermediate levels (Fig. 2E and F). This suggests that

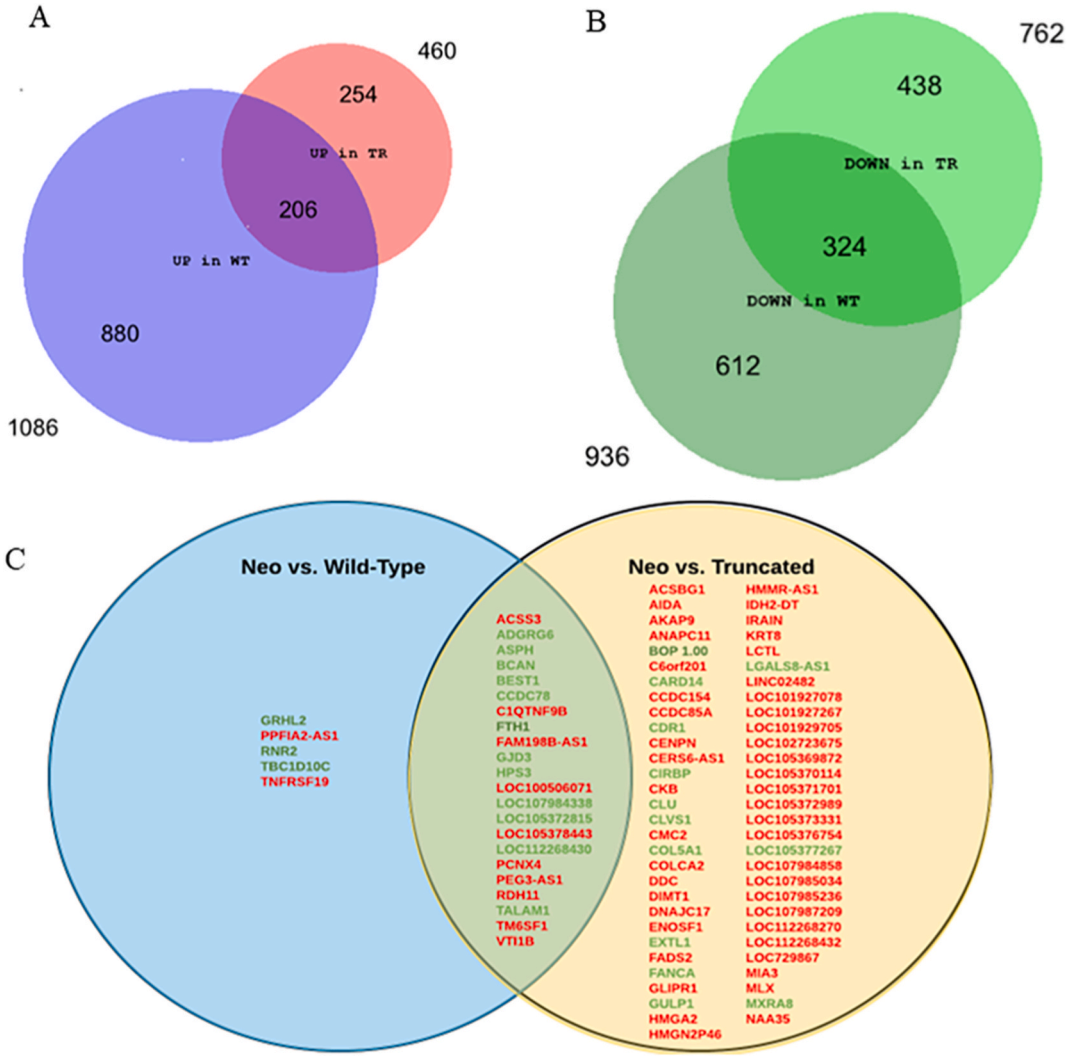

Fig. 3. RNA-Seq Reveals Upregulated and Downregulated Genes in HMGA2-WT and HMGA2-TR Cells
mRNA from LNCaP Neo, HMGA2-WT and HMGA2-TR cells was utilized to perform RNA-Seq analysis. Schematic view of data from RNA-seq from HMGA2-WT and HMGA2-TR (A) upregulated, and (B) down-regulated genes as compared to Neo. (C) Further analysis was performed using GOrilla software which revealed upregulated (red) and downregulated (green) genes. (For interpretation of the references to colour in this figure legend, the reader is referred to the Web version of this article.)

HMGA2-TR, not HMGA2-WT has an important role in promoting oxidative stress via ROS, while both HMGA2WT and to a higher extent HMGA2-TR decrease GSH:GSSG ratio indicative of reduced antioxidant capacity.

3.3. RNA-Seq reveals HMGA2-WT and TR upregulated and downregulated genes

We wanted to look further into specific pathways involved in wild-type vs truncated HMGA2 signaling. RNA-Seq analysis was performed with LNCaP Neo, LNCaP HMGA2-WT and LNCaP HMGA2-TR cells and data normalized to LNCaP Neo control cells. We created a Venn Diagram summarizing the overlap between HMGA2-WT and HMGA2-TR up-regulated genes (Fig. 3A) and down-regulated genes (Fig. 3B). In total 1086 upregulated and 936 down regulated expressed genes are detected when comparing HMGA2-WT to the Neo control whereas 460 up-regulated and 762 down-regulated genes are revealed when HMGA2-TR is compared to Neo control (Fig. 3A and B). Additionally, we utilized Gene Ontology Enrichment Analysis and Visualization Tool (Gorilla) which reveals several long non-coding RNAs that are upregulated in LNCaP HMGA2-TR cells (Fig. 3C).

3.4. RNA-seq analysis shows that truncated HMGA2 promotes oxidative stress pathways

To further investigate signaling pathway analysis, RNA-Seq data from HMGA2 isoforms individually compared to Neo control was placed into a gene set enrichment analysis (GSEA). Enrichment plots revealed that LNCaP HMGA2-TR cells has several up-regulated oxidative stress response pathways such as UV response and xenobiotic metabolism (Fig. 4A). The generation of ROS by UV radiation is one of the mechanisms through which UV light can manifest its possible detrimental effects on health [32]. Interestingly oxidative phosphorylation is shown to be up-regulated in both HMGA2-TR and HMGA2-WT when both isoforms were individually compared to Neo control (Fig. 4A and B). As expected HMGA2-WT also shows up-regulation of epithelial mesenchymal transition (EMT) which agrees with our recently published data that wild-type but not truncated HMGA2 induces EMT [25]. We further analyzed this data using Ingenuity Pathway Analysis (IPA) to determine the top canonical pathways which shows a number of pathways in common (hepatic fibrosis, axonal guidance), while some distinct in wild-type (andrenomedullin signaling) *vs.* truncated HMGA2 cells (tumor microenvironment pathway) (Table 1). Additionally, IPA analysis reveals the top up- and down-regulated genes of the two HMGA2 isoforms (Tables 2 and 3). These tables reveal that several up-regulated genes in truncated HMGA2 overexpressing cells are involved in oxidative stress, such as *SLC22A3, SEMA3A, FOXG1,* and *EYA4* (Table 2). We also utilized ingenuity pathway analysis (IPA) to predict inhibited pathways in blue and activated pathways in orange in LNCaP HMGA2-TR (Fig. 4C) and HMGA2-WT (Fig. 4D) cells that

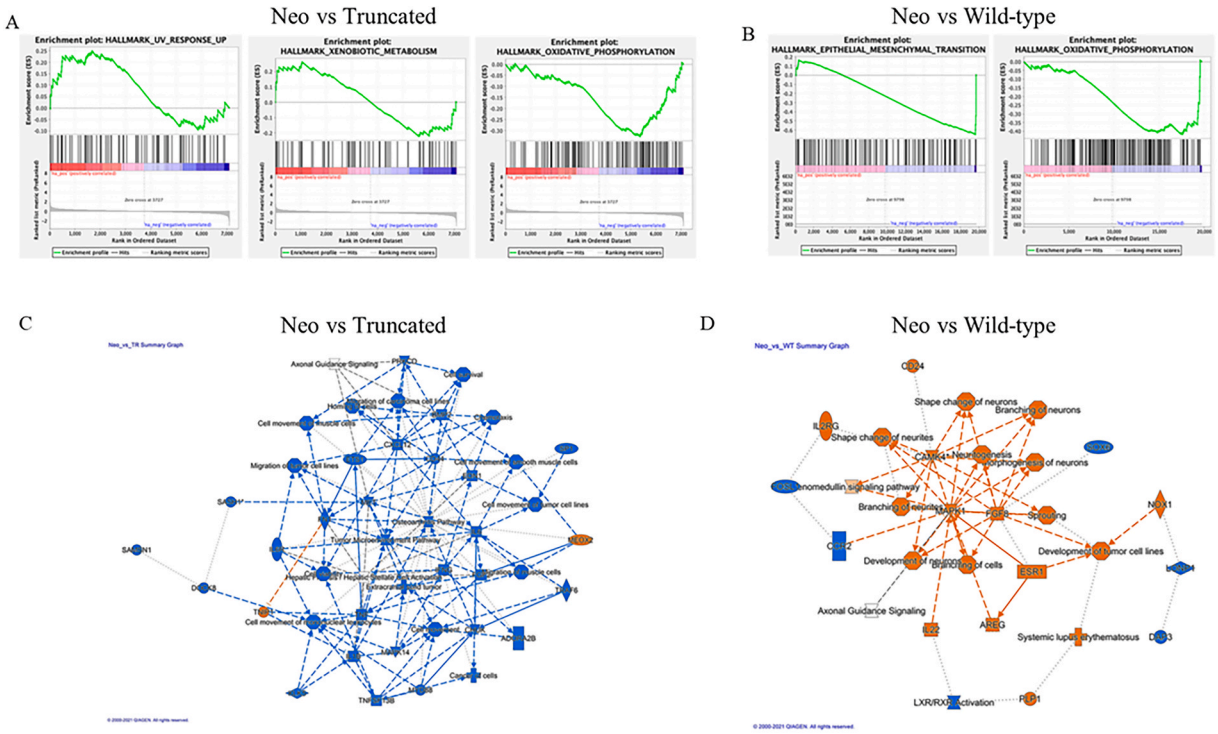

Fig. 4. RNA-Seq Reveals that Truncated HMGA2 is Involved in Oxidative Stress
Gene Set Enrichment Analysis (GSEA) of RNA-Seq data detects pathways regulated by (A) HMGA2-TR and (B) HMGA2-WT cells when compared to Neo control. Ingenuity Pathway Analysis (IPA) shows prediction of upregulated (orange) and downregulated (blue) pathways in (C) HMGA2-TR and (D) HMGA2-WT cells compared to Neo control. (For interpretation of the references to colour in this figure legend, the reader is referred to the Web version of this article.)

Table 1
Top canonical pathways of HMGA2-WT and HMGA2-TR cells compared to Neo control.

Neo vs. HMGA2-TR

Top Canonical Pathways

Name	p-value	Overlap	
Hepatic Fibrosis / Hepatic Stellate Cell Activation	4.78E-10	15.3%	29/190
Tumor Microenvironment Pathway	8.88E-08	13.5%	25/185
Axonal Guidance Signaling	4.42E-06	8.4%	42/500
Nicotine Degradation III	2.86E-05	17.7%	11/62
Osteoarthritis Pathway	3.86E-05	10.1%	23/227

1 2 3 4 5 6 7 8 9

Neo vs. HMGA2-WT

Top Canonical Pathways

Name	p-value	Overlap	
Hepatic Fibrosis / Hepatic Stellate Cell Activation	4.66E-08	17.4%	33/190
Adrenomedullin Signaling Pathway	7.40E-06	14.6%	30/205
Axonal Guidance Signaling	8.27E-06	11.2%	56/500
GP6 Signaling Pathway	1.19E-05	16.9%	22/130
Synaptogenesis Signaling Pathway	1.30E-05	12.5%	40/320

1 2 3 4 5 6 7 8 9

Table 2
Top 10 up- and down regulated genes of HMGA2-TR cells compared to Neo control.

Expr Log Ratio ↑

Molecules	Value	Chart
HMGA2	↑ 14.925	
BLOC1S5-TXNDC5	↑ 10.225	
SLC22A3	↑ 8.070	
POTEH-AS1	↑ 7.813	
KIRREL1	↑ 5.815	
CA8	↑ 5.392	
SEMA3A	↑ 5.324	
FOXG1	↑ 5.111	
EYA4	↑ 5.005	
ADGRL2	↑ 4.939	

Expr Log Ratio ↓

Molecules	Value	Chart
DCAF8L2	↓ -9.444	
AKR1C1/AKR1C2	↓ -7.717	
ALDH3A1	↓ -5.993	
AKR1C3	↓ -4.806	
URGCP-MRPS24	↓ -4.684	
CLDN1	↓ -4.387	
CXCL2	↓ -4.286	
CXCL8	↓ -4.172	
RNF17	↓ -4.005	
SMIM11B	↓ -3.983	

Table 3
Top 10 up- and down-regulated genes of HMGA2-WT compared to Neo control.

Expr Log Ratio ↑

Molecules	Value	Chart
HMGA2	↑ 13.866	
PLXDC2	↑ 11.717	
PEG10	↑ 11.704	
MAGEC1	↑ 9.526	
CBLN2	↑ 9.373	
GDF1	↑ 9.310	
POTEH-AS1	↑ 8.566	
C1RL-AS1	↑ 8.300	
TRPS1	↑ 7.879	
WLS	↑ 6.822	

Expr Log Ratio ↓

Molecules	Value	Chart
ELOVL3	↓ -10.177	
LINC01019	↓ -9.842	
DCAF8L2	↓ -9.654	
LPL	↓ -8.760	
TM4SF5	↓ -8.480	
LINC02616	↓ -7.764	
DCAF8L1	↓ -7.582	
AKR1C1/AKR1C2	↓ -6.886	
PNMA5	↓ -5.305	
LINC00632	↓ -5.264	

interestingly shows a number of neuronal pathways predicted to be upregulated in wild-type HMGA2 overexpressing cells, while a number of pathways involved in cell migration are downregulated in truncated HMGA2 overexpressing cells. Overall, truncated HMGA2 increases oxidative stress pathways.

3.5. Cytoplasmic HMGA2 interacts with oxidative stress protein, G3BP1

In order to further explore the differing roles of wild-type *vs.* truncated HMGA2, we employed a proteomics approach. Since wild-type HMGA2 is mainly nuclear, we isolated nuclear extract from LNCaP cells overexpressing HMGA2-WT and utilized this to immunoprecipitate with the HMGA2 antibody. Since truncated HMGA2 is predominantly cytoplasmic, we utilized whole cell extract from LNCaP cells overexpressing HMGA2-TR to immunoprecipitate with HMGA2 antibody. Proteomic analysis was subsequently performed to examine all HMGA2-interacting proteins. The Venn diagram shown represents some of the proteins that bind to either wild-type or truncated HMGA2 compared to IgG control (Fig. 5A) with the full list of proteins shown in Supplemental Fig. S2–S4. There were much fewer proteins bound uniquely to wild-type HMGA2 (KRT10) possibly because nuclear lysate was used, whereas whole cell lysate was used for truncated HMGA2-binding proteins, which pulled down cytoplasmic interacting proteins such as GTPase-activating protein SH3 domain-binding protein 1 (G3BP1) (Fig. 5A). We decided to focus on G3BP1 because it is a cytoplasmic stress granule protein that responds to oxidative stress [33] and our previous experiments indicate theat HMGA2 regulates oxidative stress. To confirm these findings, we first examined the basal expression of G3BP1 in LNCaP HMGA2-WT and -TR by immunofluorescence, which reveals high expression of cytoplasmic G3BP1 in LNCaP HMGA2-TR compared to HMGA2-WT (Fig. 5B). Subsequent co-immunoprecipitation with HMGA2 antibody and Western blot with G3BP1 utilizing nuclear cell extract from LNCaP HMGA2-WT or cytoplasmic fraction from LNCaP HMGA2-TR shows an interaction between G3BP1 with truncated HMGA2, but not with nuclear wild-type HMGA2 or IgG control (Fig. 5C). As a control, we repeated co-immunoprecipitation with HMGA2 antibody and Western blot with G3BP1 utilizing whole cells lysate from LNCaP HMGA2-WT cells which now showed an interaction with G3BP1 (Fig. 5C). Since LNCaP HMGA2-WT does display both cytoplasmic and nuclear HMGA2 expression as shown in Fig. 1A, the fact that there is no G3BP1 interaction with nuclear fraction but only whole cell lysate, suggests that cytoplasmic but not nuclear HMGA2 may interact with G3BP1 in LNCaP prostate cancer cells. We knocked down G3BP1 utilizing siRNA in both LNCaP HMGA2-WT and-TR cells and confirmed knockdown by immunofluorescence (Fig. 5D). Additionally, we measured ROS levels after knocking down G3BP1 in both LNCaP HMGA2-WT and -TR; results indicate that knocking down G3BP1 significantly increases ROS in the HMGA2-TR cells, while in HMGA2-WT cells ROS levels are decreased (Fig. 5E). This suggests that truncated HMGA2 may interact with stress response protein, G3BP1, to control oxidative stress which increases even more if G3BP1 is down-regulated. However, wild-type HMGA2 interaction with G3BP1 does not appear to be involved with oxidative stress.

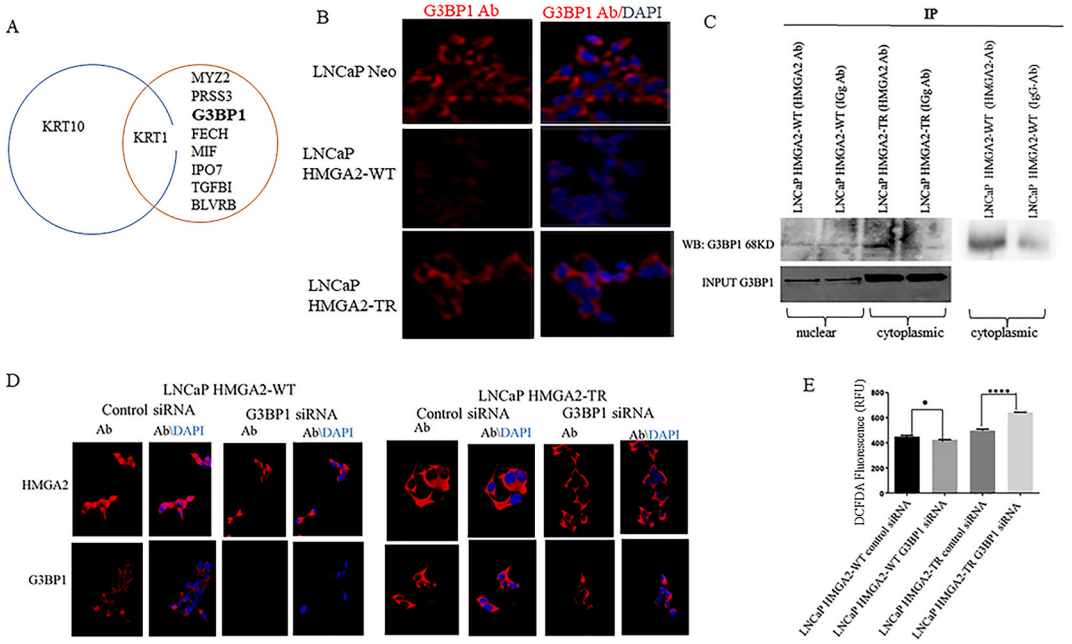

Fig. 5. G3BP1 Interacts with cytoplasmic HMGA2

(A) Nuclear fraction of HMGA2-WT cells and whole cell lysates of HMGA2-TR cells were utilized to perform immunoprecipitation (IP) with HMGA2 antibody or IgG control followed by proteomics to identify HMGA2-interacting proteins. Venn diagram represents different proteins that interact with HMGA2, but not IgG, in HMGA2-WT and HMGA2-TR cells with KRT1 common to both. (B) Immunofluorescence shows the expression of G3BP1 in LNCaP Neo, HMGA2-WT and HMGA2-TR cells. (C) We isolated nuclear fraction or whole cell lysate from HMGA2-WT cells or whole cell lysate from HMGA2-TR cells and performed IP with HMGA2 antibody or IgG control followed by Western blot with G3BP1. We performed transient knockdown of G3BP1 in HMGA2-WT and HMGA2-TR cells followed by (D) immunofluorescence with HMGA2 and G3BP1 antibody including DAPI stain for the nucleus, or (E) ROS analysis using DCFDA stain. Statistical analysis was done with GraphPad Prism; (****$p < 0.0001$, *$p < 0.05$). Bars represents SD of the mean. Magnification 40X. Results are representative of 3 independent experiments.

3.6. Truncated HMGA2 promotes sensitivity to Ferroptosis Induction that is exacerbated by G3BP1 silencing

Next, we examined whether increased ROS in HMGA2-TR cells will exhibit better responses to compounds known to be more effective in high oxidative stress environments such as ferroptosis inducer RSL3. First, LNCaP-Neo, -WT and -TR cells were treated with various doses of RSL3 for 72 h. RSL3 shows a significant decrease in cell viability only at higher concentration of 4 μM in HMGA2-TR cells compared to both HMGA2-WT and Neo control cells (Fig. 6A). However, the rate of decline in cell viability is more pronounced in HMGA2-TR cells even though at lower RSL3 concentrations, its cell viability is higher compared to LNCaP Neo and HMGA2-WT cells (Fig. 6A). HMGA2-WT shows higher sensitivity to RSL3 compared to LNCaP Neo at concentrations ranging from 0.25 to 2 μM (Fig. 6A). Ferroptosis induction by RSL3 could be reversed by ferroptosis inhibitor, ferrostatin-1 (Fer-1, Fig. 6B and C). Treatment with Fer-1 alone in LNCaP HMGA2-WT and -TR cells did not affect cell viability (Supplemental Fig. 2). Additionally, we knocked down G3BP1 in HMGA2-TR cells and confirmed knockdown by Western blot analysis (Fig. 6D). Subsequently, cells were treated with 4 μM RSL3 followed by cell viabilty assay which indicates a significant induction of ferroptosis when G3BP1 was silenced in HMGA2-TR cells and treated with RSL3 (Fig. 6E), without affecting apoptosis or increasing necrosis (Supplemental Fig. 3). Therefore, truncated HMGA2 as well as HMGA2-WT in part promotes vulnerability to ferroptosis-inducing compound RSL3, which is exacerbated by G3BP1 knockdown in HMGA2-TR cells.

3.7. Endogenous knockdown of G3BP1 and HMGA2 in PC3 cells promotes ferroptosis sensitivity

To further investigate G3BP1 and HMGA2 involvment in ferroptosis sensitively, we utilized cells with endogenous levels of G3BP1 and HMGA2. Our previous study [25] and Fig. 1A indicates predominantly high expression of truncated HMGA2 in PC3 cells. We treated PC3 cells transfected with control siRNA or HMGA2 siRNA plus DMSO, 4 μM of RSL3, or RSL3 combined ferroptosis inhibitor, ferrostatin-1 at a concentration of 1 μM followed by cell viability. There was a trend towards reduced viability with RSL3 treatment which was not significant, however, HMGA2 knockdown significantly reduced cell viability which was reversed by ferrostatin-1 (Fig. 7A). HMGA2 silencing in PC3 cells was confirmed by Western blot analysis (Fig. 7B). A similar trend was observed with G3BP1 knockdown, in which reduced cell viability was antagonized by ferrostatin-1 (Fig. 7C). G3BP1 knockdown was confirmed by Western blot analysis (Fig. 7D). Treatment with Fer-1 alone in PC3 cells did not affect cell viability (Supplemental Fig. 4). Thus, this data further confirms that HMGA2 and G3BP1 are involved in ferroptosis in PC3 cells.

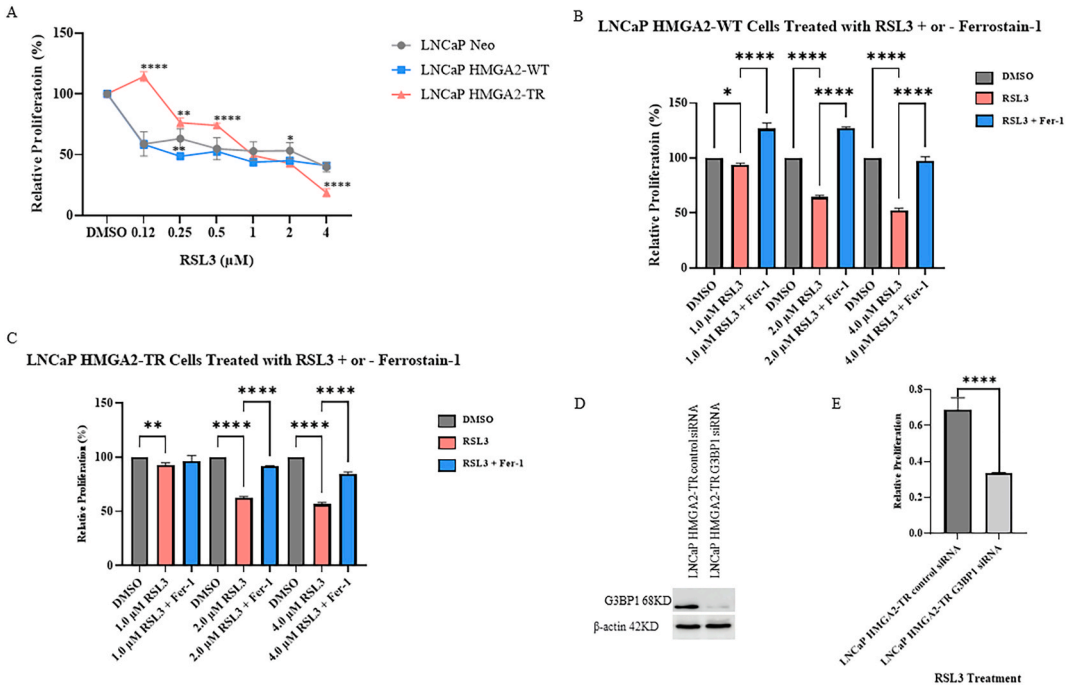

Fig. 6. Truncated HMGA2 Promotes Sensitivity to Ferroptosis Induction that is Exacerbated by G3BP1 Silencing
(A) LNCaP Neo, HMGA2-WT cells or HMGA2-TR cells were treated with various concentrations of ferroptosis inducer RSL3 for 72 h followed by cell viability analysis using MTS assay. RSL3 treatments were repeated in the presence or absence of 1 μM ferrostatin-1 and cell viability assayed in (B) HMGA2-WT cells, or (C) HMGA2-TR cells. (D) HMGA2-TR cells were treated with control or G3BP1 siRNA followed by Western blot analysis. (E) HMGA2-TR cells were co-treated with control or G3BP1 siRNA plus 4 μM RSL3 followed by MTS assay. Statistical analysis was done with GraphPad Prism; (****$p < 0.0001$, ***$p < 0.001$, **p < 0.01, *$p < 0.05$). Bars represents SD of the mean. Results are representative of 3 independent experiments.

4. Discussion

According to GLOBOCAN 2020, PCa is the most commonly diagnosed cancer in men in 112 countries including USA, while PCa accounts for the fifth most common cause for cancer death globally [34]. Mortality is largely due to metastasis, with bone being the main site of PCa metastasis [35]. HMGA2 is a non-histone protein that is up-regulated in several cancers and is associated with metastasis [36]. It is worth noting that the upregulation of HMGA2 in PCa is not a single event, but a multistep process that involves a complex interplay between genetic and epigenetic factors, leading to the progression of the disease however, several factors have been proposed. For instance epigenetic modifications such as DNA methylation and histone modifications have been proposed as mechanisms of HMGA2 upregulation in PCa [37]. Additionally, Let-7 miRNA suppresses HMGA2 expression by binding to the 3′UTR of HMGA2, and loss of Let-7 miRNA or loss of the 3′UTR in cells expressing truncated HMGA2 can lead to increased expression of HMGA2 and other oncogenic targets which leads to cancer development and progression [38]. Growth factors such as transforming growth factor-beta (TGF-β) can also transcriptionally upregulate HMGA2 [39]. Due to the rearrangement of chromosome 12 where HMGA2 is located, or alternative splicing, a new isoform of HMGA2 protein (truncated HMGA2) will arise, lacking the 3′UTR region [8,40]. We have previously shown that overexpression of truncated HMGA2 in LNCaP PCa cell lines display predominantly cytoplasmic localization, while nuclear/cytoplasmic localization is displayed in LNCaP cells overexpressing wild-type HMGA2 which promotes EMT [25]. Additionally, we published that early grade prostate cancer tissue expresses predominantly cytoplasmic HMGA2 while higher grade and metastatic tissue display more nuclear HMGA2 expression [25]. In the present study, truncated HMGA2 protein expression is detected in normal transformed prostate epithelial cells (RWPE1) and some prostate cancer cell lines, whereas wild-type HMGA2 appears to be associated with metastatic cell lines (except for C4-2), which would follow high nuclear expression of HMGA2 previously reported in bone metastatic patient tissue [25]. Interestingly, IHC staining of hyperplasia and more so chronic inflammatory prostatic tissue indicates HMGA2 staining within the cytoplasm, suggesting a possible association of cytoplasmic HMGA2 with oxidative stress. However, the Western blot in Fig. 1 with the benign prostatic fibrosis does not show high levels of truncated HMGA2, which may be because even though chronic inflammation leads to fibrosis, it is not the only contributing factor to fibrosis. A study conducted by Zong et al., reported for the first time the cytoplasmic expression of HMGA2 in normal skin tissue, while, HMGA2 translocated into the nucleus in carcinoma tissue samples [41]. Additionally, in the present study, HMGA2 mRNA and protein levels were investigated in patient tissue which shows an increase of HMGA2 wild-type and truncated isoform expression with increasing PCa gleason grade/-stage, when compared to normal prostate.

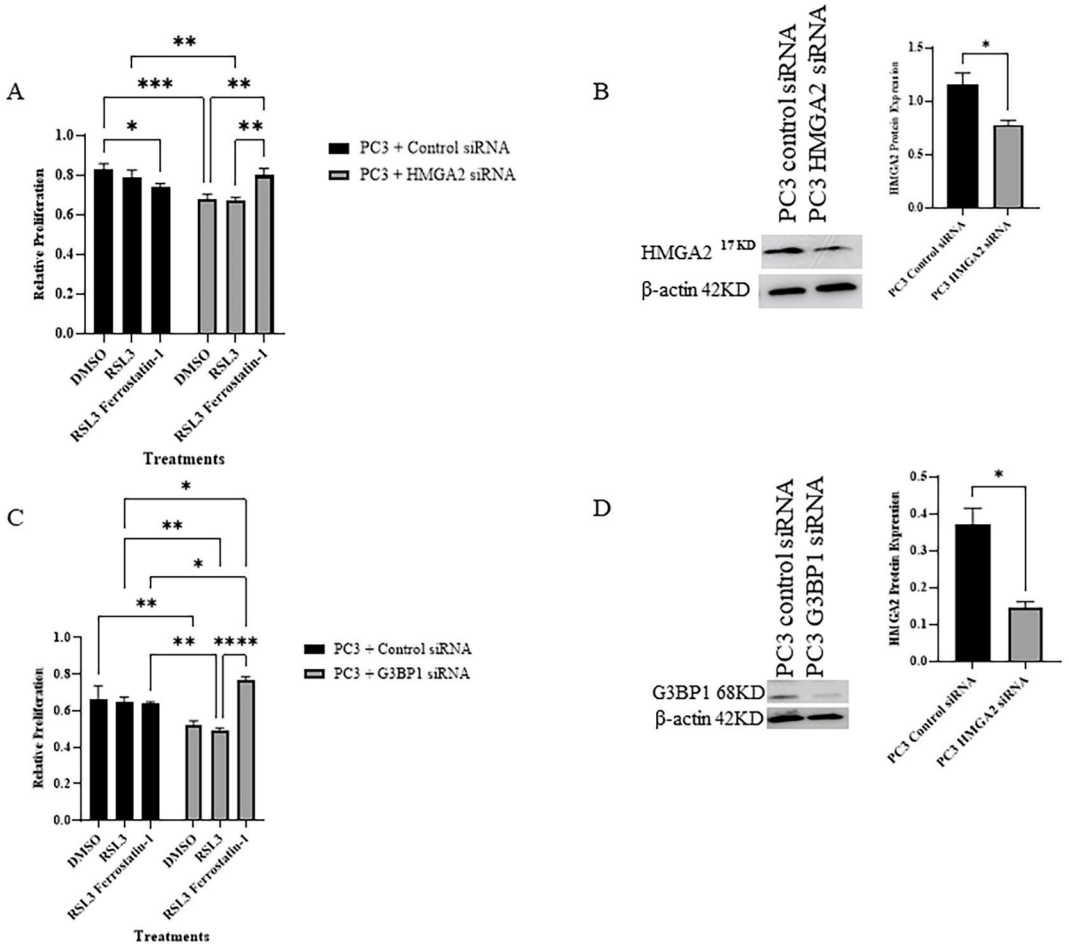

Fig. 7. Endogenous HMGA2 and G3BP1 Mediate Ferroptosis in PC3 Cells
(A) PC3 PCa cells were treated with control or HMGA2 siRNA plus or minus 4 μM RSL3 and 1 μM ferrostatin-1 for 72 h followed by cell viability analysis using MTS assay. (B) Knockdown of HMGA2 was confirmed by Western blot analysis. (C) PC3 cells were treated with control or G3BP1 siRNA plus or minus 4 μM RSL3 and 1 μM ferrostatin-1 for 72 h followed by cell viability analysis using MTS assay. (B) Knockdown of G3BP1 was confirmed by Western blot analysis. Statistical analysis was done with GraphPad Prism; (****$p < 0.0001$, ***$p < 0.001$, **$p < 0.01$, *$p < 0.05$). Bars represents SD of the mean. Results are representative of 3 independent experiments.

Next, we utilized LNCaP model overexpressing wild-type or truncated HMGA2 to delineate differential functions of wild-type *vs.* truncated HMGA2 to gain an understanding of why a prostate cancer cell would benefit from either isoform. Interestingly, LNCaP cells overexpressing truncated HMGA2 (HMGA2-TR) displays higher ROS than LNCaP cells overexpressing wild-type HMGA2 (HMGA2-WT) or empty vector Neo control cells. We observe that the antioxidant enzyme GSH and GSH/GSSG ratio were reduced in HMGA2-TR compared to Neo control cells, while the NADPH/NADP ratio is significantly higher in HMGA2-TR cells. The increased NADP/NADPH ratio could be due to higher NOX activation leading to increased ROS production as has been previously observed in platelets [42]. However, even though HMGA2-WT cells do not increase ROS, they have intermediate GSH:GSSG and NADPH:NADP ratios that are higher than Neo control but lower than HMGA2-TR cells. It is possible that the moderate levels of GSH:GSSH and NADP:NADPH are sufficient to effectively neutralize the ROS produced by the cells, leading to a decrease in overall ROS levels. However, further studies are needed to determine the exact mechanism by which ROS levels are decreased in HMGA2-WT. This data suggests that truncated HMGA2 has a more pronounced role in promoting oxidative stress compared to wild-type HMGA2.

We further investigated the differential role of wild-type *vs.* truncated HMGA2 utilizing RNA-seq analysis, which reveals several upregulated and downregulated genes. GSEA of the RNA-Seq data shows that truncated HMGA2 upregulates pathways involved in oxidative stress response. Certain oxidative stress genes uniquely upregulated by truncated HMGA2 includes *SLC22A3* which is known to facilitate heat stress-induced oxidative DNA damage [43]. Other genes upregulated by truncated HMGA2 include *SEMA3A, FOXG1,* and *EYA4.* Neurons under stressed conditions have also been shown to express *SEMA3A* and mediate microglial apoptosis [44], while *FOXG1* affects oxidative stress in OC-1 cells [45]. *EYA4*, a protein when overexpressed in mice led to apoptosis of spinal ganglion neurons and caused hearing loss, a disorder caused by increased oxidative stress [46]. The genes downregulated by truncated HMGA2 have less to do with stress; In fact, *ALDH3A1* has recently been shown to play an essential role in protecting cellular proteins against

aggregation under stress conditions [47] while *AKR1C3* has shown to be a novel EMT driver in prostate cancer metastasis through activating ERK signaling [48], and *CLDN1* promotes mesenchymal transformation in HCC cells [49]. Additionally, *CXCL2* and *CXCL8* are among the truncated HMGA2 downregulated genes that have also been shown in literature to be downregulated in an immortalized mesenchymal stem-like cell (MSC) line overexpressing truncated HMGA2 [50]. These genes are intrestingly involved in the polarization of *macrophages* toward anti-inflammatory phenotypes [51], and also contributes to tumor progression by promoting migration and invasion of cancer cells [52]. As expected RNA-Seq shows that wild-type HMGA2 upregulates the EMT pathways which agrees with our previous study that wild-type but not truncated HMGA2 promotes EMT [25]. Upregulated proteins by wild-type HMGA2 includes *PLXDC2*, which is affiliated with immune regulation [53], and PEG10, known to be involved in EMT [54]. Interestingly, both wild-type and truncated HMGA2 upregulate oxidative phosphorylation pathway. HMGA2 involvement with oxidative phosphorylation could be due to its involvement with insulin growth factor 2 mRNA binding protein 2 (IGF2BP2), a direct transcriptional target of HMGA2, which has been shown to regulate oxidative phosphorylation [55].

We report that cytoplasmic but not nuclear HMGA2 interacts with G3BP1, a cytoplasmic RNA binding protein found in stress granules (SGs) within the cytoplasm that responds to oxidative stress [56]. Interestingly, the interaction of G3BP1 with cytoplasmic HMGA2 appears to be important to control oxidative stress in cells overexpressing truncated but not wild-type HMGA2. High levels of ROS are thought to be involved in oncogenic transformation and intrestingly, due to truncated HMGA2 missing its *C*-terminus and 3′UTR, it may be more oncogenic than wild-type HMGA2. The *C*-terminus may contribute to the distinct functions seen between wild-type and truncated HMGA2. It is plausible that in response to increased oxidative stress triggered by truncated HMGA2, stress granules are formed which involves G3BP1 interacting either directly or indirectly with HMGA2 to regulate oxidative stress; this will need to be explored further. Furthermore, another protein that interacts with truncated HMGA2 from the proteomics data is protease serine 3 (PRSS3). Studies have shown that PRSS3 is up-regulated in metastatic pancreatic cancer [57] and malignant prostate cancer [58]. Our proteomic results further shows that both wild-type and truncated HMGA2 interacts with Keratin, Type I cytokeratin (KRT1) while only truncated HMGA2 interacts with Keratin, Type I Cytoskeletal 10 (KRT10) which belongs to the intermediate filament proteins that are involved in hyper-proliferative activity of cholesteatoma [59]. In ovarian cancer, overexpression of KRT10 has been associated with cisplatin-resistance by targeting PTEN in *vitro* [60] and in *vivo* [61] to overcome multi-drug resistance, so it will be informative to dissect the interaction between KRT10 and truncated HMGA2 in prostate cancer cells.

Recently, ferroptosis has gained importance as an iron-dependent programmed cell death induced by accumulation of lipid peroxidation and ROS [62,63]. High oxidative stress environment as is found in cancer promotes sensitivity to ferroptosis-inducing agents, making this a promising therapy for cancer [64]. Our data indicates that cells overexpressing truncated HMGA2 display greater vulnerability to RSL3 ferroptosis inducer, as compared to wild-type HMGA2, which can reversed by ferrostatin-1 (ferroptosis inhibitor). Literature has previously shown that stress granule protein G3BP1 interacts with cytoplasmic lncRNA P53RRA, and that this lncRNA promotes ferroptosis and apoptosis [65]. When we silienced G3BP1 in HMGA2-TR cells and treated with ferroptosis inducer RSL3, there was a greater vulnerability to ferroptosis compared to control siRNA, thus showing a new link between HMGA2, G3BP1 and ferroptosis in LNCaP cells. A limitation of our study is the detailed mechanistic interaction between HMGA2 and G3BP1. A possible mechanism could include studying GPX4, a major regulator of ferroptosis as it plays a crucial role in protecting cells from oxidative stress; studies have shown that GPX4 regulates G3BP1-mediated stress granule formation [65]. Studies have shown that GPX4 can suppress the activity of G3BP1, leading to the inhibition of cell growth and migration. [66] It is plausible that HMGA2 may regulate GPX4. This further supports the notion that interaction between truncated HMGA2 and G3BP1 in the cytoplasm may work to control elevated ROS, increasing susceptibility to ferroptosis which is further promoted by G3BP1 knockdown, this process could be downstream of GPX4 or work in a positive feedback look to carry out these complex functions. Another interesting possibility is supported by a previous study that TGF-β1can reduce the expression of xCT, a subunit of System xc− that contributes to glutathione (GSH) synthesis and protects cells against ferroptosis [67]. This study shows that TGF-β1 represses xCT expression *via* Smad3 activation, decreases GSH levels, enhances lipid peroxidation and RSL3-mediated ferroptosis in hepatocellular carcinoma cells with an early TGF-β1 signature, but not in carcinoma cells with late TGF-β1 signature that display EMT. Similar to our findings, reductions in GSH levels and increases in ROS were the largest in PLC/PRF/5 cells (41.2%) cells that represent early TGF-β1 signature but GSH decrease was more modest in Huh7 cells (26.4%) that represent late TGF-β1 signature/EMT with no effect on ROS upon TGF-β1 treatment [67]. Their explanation for the lack of increase in ROS despite partial decrease in GSH is that TGF-β1 might have induced mild oxidative stress that could be compensated by intracellular amount of GSH still present in this cell line. We can use this to similarly explain why despite some decrease in GSH in LNCaP HMGA2-WT cells (known to display EMT), there was no increase in ROS levels compared to Neo even after G3BP1 knockdown. However, LNCAP HMGA2-TR cells that do not display EMT acts like the early TGF-β1 signature whereby there is larger decrease of GSH levels accompanied by higher ROS. Overall, increased ROS in LNCaP HMGA2-TR cells make them more vulnerable to ferroptosis. Our GO analysis suggest some genes that may be involved in ferroptosis such as MXRA8 downregulated in HMGA2-TR cells; this gene has been recently associated with ferroptosis in glioma [68]. Upregulated gene ACSBG1 in HMGA2-TR cells is reported to be a pro-ferroptotic factor in heat-induced ferroptosis for cancer therapy [69]. TM6SF1 upregulated in HMGA2-TR cells is shown to be a ferroptosis related gene in lung adenocarcinoma [70]. FTH1 gene is downregulated in both HMGA2-WT and -TR cells; this encodes a member of ferritin that is an iron storage and antioxidant molecule and regulates ferroptosis [68,71]. Thus ferroptosis inducers could be a possible therapy for prostate cancer cells overexpressing truncated HMGA2. Of note, HMGA2-WT cells were also vulnerable to ferroptosis when compared to Neo control cells, that may be linked to their intermediate decrease in GSH:GSSG ratio that was lower than Neo, but not HMGA2-TR cells. Therefore, wild-type HMGA2 may also contribute sensitivity to ferroptosis to a lesser degree.

To validate using PC3 cells that is published to endogenously express high levels of truncated HMGA2, RSL3 treatment led to a slight but not significant decrease in cell viability, however, knockdown of HMGA2 or G3BP1 decreased cell viability significantly

which was restored by co-treatment with RSL3 and ferrostatin-1, confirming the role of these proteins in ferroptosis. A previous study reveled that providing reduced glutathione or the radical-trapping antioxidant ferrostatin-1 to ferroptotic dying cells can rescue and promote their recovery [72]. Recently, data supports induction of ferroptosis as a new therapeutic strategy for advanced prostate cancer as a monotherapy and in combination with second-generation antiandrogens such as enzalutamide [22].

Overall, this study is the first to perform a comprehensive analysis of the mechanistic function of wild-type *vs.* truncated HMGA2 in prostate cancer. We reveal that truncated HMGA2 can increase oxidative stress more than wild-type HMGA2; both isoforms interact with stress protein, G3BP1 within the cytoplasm; and both isoforms decrease GSH:GSSG ratio. This confers vulnerability to ferroptosis, more so in cells expressing truncated HMGA2 that display higher levels of HMGA2, higher ROS and lower antioxidant status compared to wild-type HMGA2 cells. This novel pathway reveals prostate cancer patients who overexpress HMGA2 associated with increased oxidative stress may be more sensitive to ferroptosis and offers ferroptosis inducers as a possible therapeutic approach for patients overexpressing HMGA2.

Author contribution statement

Taaliah Campbell, Ohuod Hawsawi: Performed the experiments; Analyzed and interpreted the data; Wrote the paper.

Veronica Henderson; Precious Dike, Bor-Jang Hwang, Yusuf Liadi, ElShaddai Z. White, Jin Zou: Performed the experiments.

GuangDi Wang, Qiang Zhang, Derrick Scott, Nathan Bowen: Analyzed and interpreted the data; Contributed reagents, materials, analysis tools or data.

Cimona V. Hinton: Analyzed and interpreted the data.

Valerie Odero-Marah: Conceived and designed the experiments; Analyzed and interpreted the data; Contributed reagents, materials, analysis tools or data; Wrote the paper.

Funding statement

Valerie Odero-Marah was supported by National Institute on Minority Health and Health Disparities [2U54MD007590 & U54MD013376].

GuangDi Wang was supported by National Institute on Minority Health and Health Disparities [5U54MD007595].

Taaliah Campbell was supported by National Institute of General Medical Sciences [5R25GM060414].

Data availability statement

Data included in article/supplementary material/referenced in article.

Declaration of competing interest

The authors have no competing interests and nothing to declare.

Acknowledgements

We are grateful to Nebraska Medicine Fred & Pamela Buffett Cancer Center and Dr. Pankaj Singh (University of Nebraska Medical Center) for the metabolomics analysis.

Appendix A. Supplementary data

Supplementary data related to this article can be found at https://doi.org/10.1016/j.heliyon.2023.e14810.

References

1 A.R. Young, M. Narita, Oncogenic HMGA2: short or small? Genes Dev. 21 (2007) 1005–1009.
2 M.F. Shannon, L.S. Coles, J. Attema, P. Diamond, The role of architectural transcription factors in cytokine gene transcription, J. Leukoc Biol. 69 (2001) 21–32.
3 N. Abe, et al., An increased high-mobility group A2 expression level is associated with malignant phenotype in pancreatic exocrine tissue, Br. J. Cancer 89 (2003) 2104.
4 B. Meyer, et al., HMGA2 overexpression in non-small cell lung cancer, Mol. Carcinog. 46 (2007) 503–511.
5 J. Miyazawa, A. Mitoro, S. Kawashiri, K.K. Chada, K. Imai, Expression of mesenchyme-specific gene HMGA2 in squamous cell carcinomas of the oral cavity, Cancer Res. 64 (2004) 2024–2029.
6 R. Sgarra, et al., Nuclear phosphoproteins HMGA and their relationship with chromatin structure and cancer, FEBS Lett. 574 (2004) 1–8.
7 S. Battista, et al., The expression of a truncated HMGI-C gene induces gigantism associated with lipomatosis, Cancer Res. 59 (1999) 4793–4797.
8 M. Cesana, et al., A CLK3-HMGA2 Alternative splicing axis impacts human hematopoietic stem cell molecular identity throughout development, Cell Stem Cell 22 (2018) 575–588 e577, https://doi.org/10.1016/j.stem.2018.03.012.
9 D.S. Hunter, et al., Aberrant expression of HMGA2 in uterine leiomyoma associated with loss of TSC2 tumor suppressor gene function, Cancer Res. 62 (2002) 3766–3772.

10 M.D. Odero, et al., Disruption and aberrant expression of HMGA2 as a consequence of diverse chromosomal translocations in myeloid malignancies, Leukemia 19 (2005) 245.
11 B. Uttara, A.V. Singh, P. Zamboni, R. Mahajan, Oxidative stress and neurodegenerative diseases: a review of upstream and downstream antioxidant therapeutic options, Curr. Neuropharmacol. 7 (2009) 65–74.
12 T.D. Oberley, W. Zhong, L.I. Szweda, L.W. Oberley, Localization of antioxidant enzymes and oxidative damage products in normal and malignant prostate epithelium, Prostate 44 (2000) 144–155.
13 X.-Y. Sun, S.P. Donald, J.M. Phang, Testosterone and prostate specific antigen stimulate generation of reactive oxygen species in prostate cancer cells, Carcinogenesis 22 (2001) 1775–1780.
14 J.P.T. Ward, From Physiological redox signalling to oxidant stress, Adv. Exp. Med. Biol. 967 (2017) 335–342, https://doi.org/10.1007/978-3-319-63245-2_21.
15 R. Sohal, L. Arnold, W.C. Orr, Effect of age on superoxide dismutase, catalase, glutathione reductase, inorganic peroxides, TBA-reactive material, GSH/GSSG, NADPH/NADP+ and NADH/NAD+ in Drosophila melanogaster, Mech. Ageing Dev. 56 (1990) 223–235.
16 O. Zitka, et al., Redox status expressed as GSH: GSSG ratio as a marker for oxidative stress in paediatric tumour patients, Oncol. Lett. 4 (2012) 1247–1253.
17 H. Mahboubi, U. Stochaj, Cytoplasmic stress granules: dynamic modulators of cell signaling and disease, Biochim. Biophys. Acta Mol. Basis Dis. 1863 (2017) 884–895, https://doi.org/10.1016/j.bbadis.2016.12.022.
18 Y. Wang, et al., The interaction of YBX1 with G3BP1 promotes renal cell carcinoma cell metastasis via YBX1/G3BP1-SPP1- NF-kappaB signaling axis, J. Exp. Clin. Cancer Res. 38 (2019) 386, https://doi.org/10.1186/s13046-019-1347-0.
19 Y. Mou, et al., Ferroptosis, a new form of cell death: opportunities and challenges in cancer, J. Hematol. Oncol. 12 (2019) 34, https://doi.org/10.1186/s13045-019-0720-y.
20 J. Li, et al., Ferroptosis: past, present and future, Cell Death Dis. 11 (2020) 88, https://doi.org/10.1038/s41419-020-2298-2.
21 J. Liu, R. Kang, D. Tang, Signaling pathways and defense mechanisms of ferroptosis, FEBS J. (2021), https://doi.org/10.1111/febs.16059.
22 A. Ghoochani, et al., Ferroptosis inducers are a novel therapeutic approach for advanced prostate cancer, Cancer Res. 81 (2021) 1583–1594, https://doi.org/10.1158/0008-5472.CAN-20-3477.
23 H. Yamaguchi, et al., Caspase-independent cell death is involved in the negative effect of EGF receptor inhibitors on cisplatin in non-small cell lung cancer cells, Clin. Cancer Res. 19 (2013) 845–854, https://doi.org/10.1158/1078-0432.CCR-12-2621.
24 L. Chen, et al., Erastin sensitizes glioblastoma cells to temozolomide by restraining xCT and cystathionine-gamma-lyase function, Oncol. Rep. 33 (2015) 1465–1474, https://doi.org/10.3892/or.2015.3712.
25 O. Hawsawi, et al., High mobility group A2 (HMGA2) promotes EMT via MAPK pathway in prostate cancer, Biochem. Biophys. Res. Commun. 504 (2018) 196–202.
26 O. Hawsawi, et al., High mobility group A2 (HMGA2) promotes EMT via MAPK pathway in prostate cancer, Biochem. Biophys. Res. Commun. 504 (2018) 196–202, https://doi.org/10.1016/j.bbrc.2018.08.155.
27 S. Bajad, V. Shulaev, LC-MS-based metabolomics, Methods Mol. Biol. 708 (2011) 213–228, https://doi.org/10.1007/978-1-61737-985-7_13.
28 J. Xia, R. Mandal, I.V. Sinelnikov, D. Broadhurst, D.S. Wishart, MetaboAnalyst 2.0—a comprehensive server for metabolomic data analysis, Nucleic acids Res. 40 (2012) W127–W133.
29 J. Dougan, et al., Proteomics-metabolomics combined approach identifies peroxidasin as a protector against metabolic and oxidative stress in prostate cancer, Int. J. Mol. Sci. 20 (2019), https://doi.org/10.3390/ijms20123046.
30 L.J. Burton, et al., Muscadine grape skin extract induces an unfolded protein response-mediated autophagy in prostate cancer cells: a TMT-based quantitative proteomic analysis, PLoS One 11 (2016), e0164115, https://doi.org/10.1371/journal.pone.0164115.
31 L.J. Burton, et al., Muscadine grape skin extract can antagonize Snail-cathepsin L-mediated invasion, migration and osteoclastogenesis in prostate and breast cancer cells, Carcinogenesis 36 (2015) 1019–1027.
32 T.L. de Jager, A.E. Cockrell, S.S. Du Plessis, Ultraviolet light induced generation of reactive oxygen species, Adv. Exp. Med. Biol. 996 (2017) 15–23, https://doi.org/10.1007/978-3-319-56017-5_2.
33 P. Anderson, N. Kedersha, P. Ivanov, Stress granules, P-bodies and cancer, Biochim. Biophys. Acta (BBA)-Gene Regul. Mech. 1849 (2015) 861–870.
34 H. Sung, et al., Global Cancer Statistics 2020: GLOBOCAN estimates of incidence and mortality worldwide for 36 cancers in 185 countries, CA Cancer J. Clin. 71 (2021) 209–249, https://doi.org/10.3322/caac.21660.
35 R.L. Siegel, K.D. Miller, A. Jemal, Cancer statistics, 2020, CA Cancer J. Clin. 70 (2020) 7–30, https://doi.org/10.3322/caac.21590.
36 A. Fusco, M. Fedele, Roles of HMGA proteins in cancer, Nat. Rev. Cancer 7 (2007) 899.
37 K.P. Keil, C.M. Vezina, DNA methylation as a dynamic regulator of development and disease processes: spotlight on the prostate, Epigenomics 7 (2015) 413–425, https://doi.org/10.2217/epi.15.8.
38 U. Unachukwu, K. Chada, J. D'Armiento, High mobility group AT-Hook 2 (HMGA2) oncogenicity in mesenchymal and epithelial neoplasia, Int. J. Mol. Sci. 21 (2020), https://doi.org/10.3390/ijms21093151.
39 B. Mansoori, et al., HMGA2 as a critical regulator in cancer development, Genes (Basel) 12 (2021), https://doi.org/10.3390/genes12020269.
40 K. Ikeda, P.J. Mason, M. Bessler, 3′ UTR-truncated Hmga2 cDNA causes MPN-like hematopoiesis by conferring a clonal growth advantage at the level of HSC in mice, Blood 117 (2011) 5860–5869.
41 Y. Li, et al., Hmga2 translocation induced in skin tumorigenesis, Oncotarget 8 (2017), 30019.
42 E. Hosseini, M. Ghasemzadeh, M. Atashibarg, M. Haghshenas, ROS scavenger, N-acetyl-l-cysteine and NOX specific inhibitor, VAS2870 reduce platelets apoptosis while enhancing their viability during storage, Transfusion 59 (2019) 1333–1343, https://doi.org/10.1111/trf.15114.
43 J.X. Xiong, et al., Epigenetic alterations of a novel antioxidant gene SLC22A3 predispose susceptible individuals to increased risk of esophageal cancer, Int. J. Biol. Sci. 14 (2018) 1658–1668, https://doi.org/10.7150/ijbs.28482.
44 H.H. Majed, et al., A novel role for Sema3A in neuroprotection from injury mediated by activated microglia, J. Neurosci. 26 (2006) 1730–1738, https://doi.org/10.1523/JNEUROSCI.0702-05.2006.
45 Z.H. He, et al., The nuclear transcription factor FoxG1 affects the sensitivity of mimetic aging hair cells to inflammation by regulating autophagy pathways, Redox. Biol. 28 (2020), 101364, https://doi.org/10.1016/j.redox.2019.101364.
46 K.N. Prasad, S.C. Bondy, MicroRNAs in hearing disorders: their regulation by oxidative stress, inflammation and antioxidants, Front. Cell Neurosci. 11 (2017) 276, https://doi.org/10.3389/fncel.2017.00276.
47 G.P. Voulgaridou, et al., Human aldehyde dehydrogenase 3A1 (ALDH3A1) exhibits chaperone-like function, Int. J. Biochem. Cell. Biol 89 (2017) 16–24, https://doi.org/10.1016/j.biocel.2017.05.017.
48 B. Wang, et al., AKR1C3, a crucial androgenic enzyme in prostate cancer, promotes epithelial-mesenchymal transition and metastasis through activating ERK signaling, Urol. Oncol. 36 (2018) 472.e411–472.e420, https://doi.org/10.1016/j.urolonc.2018.07.005.
49 Y. Suh, et al., Claudin-1 induces epithelial-mesenchymal transition through activation of the c-Abl-ERK signaling pathway in human liver cells, Oncogene 36 (2017) 1167–1168, https://doi.org/10.1038/onc.2016.294.
50 J. Henriksen, et al., Identification of target genes for wild type and truncated HMGA2 in mesenchymal stem-like cells, BMC Cancer 10 (2010) 329, https://doi.org/10.1186/1471-2407-10-329.
51 D. Di Mitri, et al., Re-education of tumor-associated macrophages by CXCR2 blockade drives senescence and tumor inhibition in advanced prostate cancer, Cell. Rep. 28 (2019) 2156–2168.e2155, https://doi.org/10.1016/j.celrep.2019.07.068.
52 M. Hosono, et al., CXCL8 derived from tumor-associated macrophages and esophageal squamous cell carcinomas contributes to tumor progression by promoting migration and invasion of cancer cells, Oncotarget 8 (2017) 106071–106088, https://doi.org/10.18632/oncotarget.22526.
53 ....
54 M. Zhang, et al., PEG10 is imperative for TGF-β1-induced epithelial-mesenchymal transition in hepatocellular carcinoma, Oncol. Rep. 37 (2017) 510–518, https://doi.org/10.3892/or.2016.5282.

55 M. Janiszewska, et al., Imp2 controls oxidative phosphorylation and is crucial for preserving glioblastoma cancer stem cells, Genes Dev. 26 (2012) 1926–1944, https://doi.org/10.1101/gad.188292.112.
56 L. Chen, B. Liu, Relationships between stress granules, oxidative stress, and neurodegenerative diseases, Oxid. Med. Cell. Long. 2017 (2017).
57 G. Jiang, et al., PRSS3 promotes tumour growth and metastasis of human pancreatic cancer, Gut 59 (2010) 1535–1544.
58 A. Hockla, et al., PRSS3/mesotrypsin is a therapeutic target for metastatic prostate cancer, Mol. Cancer Res. 10 (2012) 1555–1566.
59 E. Olszewska, H. Sudhoff, Comparative cytokeratin distribution patterns in cholesteatoma epithelium, Histol. Histopathol. 22 (2007) 37–42.
60 H. Wu, K. Wang, W. Liu, Q. Hao, PTEN overexpression improves cisplatin-resistance of human ovarian cancer cells through upregulating KRT10 expression, Biochem. Biophys. Res. Commun. 444 (2014) 141–146.
61 H. Wu, K. Wang, W. Liu, Q. Hao, Recombinant adenovirus-mediated overexpression of PTEN and KRT10 improves cisplatin resistance of ovarian cancer in vitro and in vivo, Genet. Mol. Res. 14 (2015) 6591–6597.
62 B.R. Stockwell, et al., Ferroptosis: a regulated cell death nexus linking metabolism, redox biology, and disease, Cell 171 (2017) 273–285, https://doi.org/10.1016/j.cell.2017.09.021.
63 W.S. Yang, et al., Peroxidation of polyunsaturated fatty acids by lipoxygenases drives ferroptosis, Proc. Natl. Acad. Sci. USA 113 (2016) E4966–4975, https://doi.org/10.1073/pnas.1603244113.
64 C.M. Bebber, F. Muller, L. Prieto Clemente, J. Weber, S. von Karstedt, Ferroptosis in cancer cell biology, Cancers (Basel) 12 (2020), https://doi.org/10.3390/cancers12010164.
65 C. Mao, et al., A G3BP1-interacting lncRNA promotes ferroptosis and apoptosis in cancer via nuclear sequestration of p53, Cancer Res. 78 (2018) 3484–3496, https://doi.org/10.1158/0008-5472.CAN-17-3454.
66 B. Xie, Y. Guo, Molecular mechanism of cell ferroptosis and research progress in regulation of ferroptosis by noncoding RNAs in tumor cells, Cell Death Discov. 7 (2021) 101, https://doi.org/10.1038/s41420-021-00483-3.
67 D.H. Kim, W.D. Kim, S.K. Kim, D.H. Moon, S.J. Lee, TGF-beta1-mediated repression of SLC7A11 drives vulnerability to GPX4 inhibition in hepatocellular carcinoma cells, Cell Death Dis. 11 (2020) 406, https://doi.org/10.1038/s41419-020-2618-6.
68 Z. Xu, X. Chen, L. Song, F. Yuan, Y. Yan, Matrix Remodeling-associated protein 8 as a novel indicator contributing to glioma immune response by regulating ferroptosis, Front. Immunol. 13 (2022), 834595, https://doi.org/10.3389/fimmu.2022.834595.
69 S. Xie, et al., Metabolic control by heat stress determining cell fate to ferroptosis for effective cancer therapy, ACS Nano 15 (2021) 7179–7194, https://doi.org/10.1021/acsnano.1c00380.
70 Z. Feng, et al., Identification and validation of a GPX4-related immune prognostic signature for lung adenocarcinoma, J. Oncol. 2022 (2022), 9054983, https://doi.org/10.1155/2022/9054983.
71 M. Di Sanzo, B. Quaresima, F. Biamonte, C. Palmieri, M.C. Faniello, FTH1 pseudogenes in cancer and cell metabolism, Cells 9 (2020), https://doi.org/10.3390/cells9122554.
72 H.M. Tang, H.L. Tang, Cell recovery by reversal of ferroptosis, Biol. Open 8 (2019), https://doi.org/10.1242/bio.043182.